

Review

# Peculiar Magnetic Features and Superconductivity in Sulfur Doped Amorphous Carbon

Israel Felner

Racah Institute of Physics, The Hebrew University, Jerusalem 91904, Israel; israela@vms.huji.ac.il;  
Tel.: +972-2-6585752

Academic Editor: Carlos J. Gómez García

Received: 3 August 2016; Accepted: 30 August 2016; Published: 13 September 2016

**Abstract:** We report on magnetic studies of inhomogeneous commercial and synthesized amorphous carbon (a-C) and a-C doped with sulfur (a-CS) powders which exhibit (i) peculiar magnetic behavior and (ii) traces of two superconducting (SC) phases  $T_C \sim 33$  and at 65 K. (i) The temperature dependence of zero-field-cooled (ZFC) curves measured up to room temperature show well distinguished elusive peaks at around 50–80 K, and their origin is not yet known. These peaks are totally washed-out in the second ZFC sweeps and in the FC branches as well. As a result, in the vicinity of the peaks, the FC curves lie below the ZFC peaks ( $FC < ZFC$ ), a phenomenon which is rarely observed. These magnetic anomalies are intrinsic properties of a-C and a-CS materials (ii) SC was observed in three different a-C sources: (a) The commercial a-C powder contains 0.21% of sulfur and it is suggested that two different a-CS phases (at 33 and 65 K) are the origin of the two SC states observed. The compositions of these two phases are not yet unknown. The small SC volume fractions of the 33 K phase can be enhanced by a solid reaction with additional sulfur at 250 °C; (b) the synthesized (a-C) powder (obtained from decomposition of sucrose) is not SC. However, when mixed with sulfur and heated at 400 °C under a protective atmosphere, the a-CS powder obtained also show traces of a SC phase at  $T_C = 42$  K; (c) The same occurs in a-C thin films. The as-grown films are not SC but a SC phase at  $T_C = 34$  K emerges after the films were reacted with sulfur at elevated temperatures. It is concluded, therefore, that all SC phases observed are due to different unknown a-CS phases. Since the a-C and a-CS powders possess SC and magnetic states, we believe that these powders resemble the high  $T_C$  curates and Fe-As based systems in which the SC and the magnetic states are closely related to each other.

**Keywords:** amorphous carbon; superconductivity; peculiar magnetic behavior

## 1. Introduction

Interest in magnetic nano-sized particles has increased in the last few years by virtue of their potential for application. These materials with dimensions intermediate between molecules and bulk solids are intriguing due to their novel electronic features which depend on the particle size, topology, surface conditions, etc. Amorphous carbon (a-C) is a good example of this kind of materials. Its graphitized carbon fragments have a very large surface area and possess both negative and positive curvatures. The most common polymorphs of carbon are: (i) graphite in which the  $sp^2$  hybridization (band gap  $E_g \approx 0.1$  eV) forms hexagonal and rhombohedral stacking orders [1] and (ii) diamond in which  $sp^3$  carbons (band gap  $E_g = 5.4$  eV) form a three-dimensional lattice of cubic symmetry. Changing the  $sp^2/sp^3$  ratio may tune the band gap between that of diamond and graphite.

Ferromagnetism (FM) is typically the property of transition and/or rare-earth metals, alloys and inter-metallic compounds, with unpaired electrons in unfilled atomic shells. On the other hand, carbon atoms show a very strong tendency to pair up their outer-shell electrons in covalent bonds. Nevertheless, various forms of carbon systems have recently been found to exhibit a FM or a FM-like

behavior. Because of the features mentioned above, a-C is also a promising candidate for searching for new superconducting (SC) materials [2,3].

The magnetic properties of two a-C sources have been extensively studied and reported [4]: (a) A inhomogeneous *commercial* Fisher powder dated from 1935 and (b) *fabricated* a-C powder obtained by multi-stage melting of ultra-pure sucrose ( $C_{12}H_{22}O_{11}$ ). (a) Energy dispersive spectroscopy (EDS) study proved that the commercial powder contains: tiny amounts of sulfur ( $\sim 0.21$  at %),  $\sim 360$  ppm of ferri-magnetic magnetite ( $Fe_3O_4$ )  $T_M = 853$  K) and also other paramagnetic (PM) ions such as Ni and Mn. Due to its inhomogeneity, the extensive zero-field-cooled (ZFC) and field-cooled (FC) magnetic studies exhibit scatter results. (i) Most of the samples presented the ferri-magnetic behavior of magnetite, and at low temperatures, the PM ions' contribution; (ii) A few samples exhibited well-observed magnetic peaks (at 50–80 K) in their first ZFC curves; (iii) The rest showed traces of two SC phases with  $T_C$  around 33 and 65 K. Heating these powders with sulfur (a-CS) at elevated temperatures did not change much their sulfur concentration but increased the amplitude of the ZFC peaks and the SC volume fraction of the lower SC phase [3]; (b) The fabricated a-C virgin powder is essentially diamagnetic, does not contain sulfur and has much less  $Fe_3O_4$  and PM impurities. The same three magnetic phenomena have been observed when this powder was doped with sulfur at elevated temperatures.

*Superconductivity:* The search for SC in carbon-based materials (CBM) triggered a large number of studies in recent years. Most of the research was done on intercalated graphite compounds in which foreign atoms were inserted between the two-dimensional hexagonal sheets of graphite. For example:  $KC_8$  ( $T_c = 0.15$  K) [5], and  $CaC_6$  ( $T_c = 11.5$  K) [6]. Much higher  $T_c$  values were obtained in alkali doped fullerenes  $C_{53}C_{60}$  ( $T_c = 38$  K) [7] and in inter-halogen-doped fullerenes ( $T_c > 60$  K) [8]. Inhomogeneous SC at 35 K was obtained at the surface of sulfur-graphite composites [9]. Since graphite and fullerene ( $C_{60}$ ) are not superconducting, it was suggested that the transfer of charges from the alkali metals to the graphite (or fullerenes) plays an important role in the appearance of the SC state. A comprehensive review on SC in CBM can be found in the literature [10]. However, the simple models existing until now are insufficient to predict the appearance and the magnitude of  $T_c$  in these alkali-intercalated materials.

As mentioned above, traces of SC two SC phases (up to 65 K) were detected in two different commercial a-C powders. SC at ( $T_c = 34$  K) was also observed in a-C thin films prepared by Electron-Beam Induced Deposition (EBID) after they were synthesized with sulfur at 250 °C. Since in all three cases SC in a-C was observed only when the powders were exposed to sulfur, it is believed sulfur is essential to the existence of the SC state in all a-C materials. Due to the fact that the SC states already observed are not bulk properties, the exact composition of these phases are as yet unknown. All those experiments agree well with theoretical expectations, which predict that intercalated sulfur and structural disorder can locally induce extra carriers into graphite/graphene sheets and therefore induce or enhance the SC state [11].

The most exciting recent observations in high temperature superconductivity (HTSC) are the new experimental and theoretical results of  $H_2S$  samples measured under high pressures [12]. SC at  $T_c = 203$  K was directly proven by resistivity measurements followed by a Meissner effect study. It is clearly evidenced that under high pressure  $H_2S$  decomposed to  $H_3S$  which is supposed to be the SC phase. The isotope effect in  $H_3S$  provided direct evidence for the conventional phonon mediated pairing. Thus, the common denominator in both a-C ( $T_c \approx 67$  K at ambient pressure) and  $H_3S$  ( $T_c = 203$  K under  $\sim 200$  GPa) systems is sulfur which possibly may serve as the basic crucial ingredient in these new HTSC classes. This similarity will be further discussed in the last section.

*Peculiar magnetic behavior:* The magnetic features of amorphous systems are mainly controlled by the disorder state, which affects the temperature dependence of their ZFC and FC branches. Microscopically, disorder may change the extent of the wave function and as a result the change from extended wave function to localized states. On the other hand, impurities, structural disorder and/or topological defects may tune the amorphous disordered nature to slightly ordered states [13]. Indeed, a FM state in CBM was achieved by proton irradiation [14], by adsorbed foreign atoms such as hydrogen [15] and/or oxygen [16]. Ferromagnetism was also observed in graphitic sheets with positive

or negative curvatures [17], in fullerene-related carbon [18], in carbon nano-spheres encapsulating silver nanoparticles [19], and in carbon nano-foam (CNF). The CNF powder has a high surface area and display peaks in the ZFC branches only immediately after their synthesis. They disappear a very short time later [20–22]. Recently, magnetization was induced in Cu/C<sub>60</sub> interfaces [23], and strongly spin-polarized interfaces at room temperature in ultra-thin a-C layers on FM cobalt have been reported [24]. In addition, scanning tunneling microscopy (STM) results showed that biological retinoic acid (which comprising only carbon, oxygen and hydrogen atoms) physically adsorbed on an inert gold surface may exhibit a localized magnetic state [25]. Despite the accumulated growing evidence of FM or FM-like states in CBM, the crucial factors that stabilize them are still unclear.

Similarly to CNF, unexpectedly in several a-CS samples, two intrinsic anomalies were observed. First, peaks were observed in the ZFC branches and around their positions the ZFC curves were much higher than the FC ones (ZFC > FC). Second, these peaks are elusive and disappear in the second ZFC as well as in the FC runs. The two anomalies are connected to each other and a qualitative model to explain them is given in the discussion section.

In this paper, we review the most prominent magnetic measurements performed on selected a-C and a-CS samples which exhibit traces of SC and/or unusual magnetic behavior. In addition to the already published data [4], we present here new unpublished results. This manuscript is divided into two major parts. Following the experimental details section, we present first the SC states observed in commercial and fabricated a-C powders, as well as in sulfur doped a-C thin-films. Next, we describe the unusual magnetic features of several a-C and a-CS materials and mention similar observations in two other unrelated systems. For the sake of clarity, the various samples studied and their necessary characteristic features are listed in Table 1.

**Table 1.** Details on the a-C and a-CS materials report here.

Compound	Heat Treatment at °C	Displayed in Figure	Magnetic Behavior
Commercial a-C	800	1 and 9	Verwey transition
Commercial a-C sample 6	pristine	2	Normal
Commercial a-C Sample 13	pristine	3	Normal (ZFC curves overlap)
Commercial a-C Sample 1	pristine	4	SC at 33(1) and 64(1) K
Commercial a-C Sample 13	pristine	5	SC at 65(1) K
Commercial a-CS	250	6	SC at 38(1) K
Fabricated a-C	-	7	blank
Fabricated a-CS	400	7	SC at 42(1) K
a-C Thin film +S	250	8	SC at 34(1) K
Commercial a-C Sample 6	pristine	10	Peak in the ZFC plot at 80 K
Commercial a-C Sample 5	pristine	11	ZFC > FC
Commercial a-CS Sample 1 part-1	400	12	Peak in the ZFC plot at 78 K (ZFC > FC)
Commercial a-CS Sample 1 part-1	400	13	H = 1 kOe ZFC = FC
Commercial a-CS Sample 1 part-1	400	14	ZFC > FC
Fabricated a-C Sample 1 part 3	400	15	Peak in the ZFC plot at 52 K (ZFC > FC)
Fabricated a-C Sample 4 part 3	400	16	Reappearance of the ZFC after 18 months
Commercial a-CB	400	17	Peak in the ZFC plot at 63 K (ZFC > FC)
Crystalline graphite	-	18	No features

## 2. Experimental Details.

The commercial a-C powder was a-C fabricated by Fisher (C190-N) in 1935. First, a-C sample was heated to 800 °C (assign as a-C800) and then cooled to ambient temperature. Second, other non-commercial a-C sources were obtained by multi-stage pyrolytic thermal treatment (up to 650 °C) of pure sucrose (C<sub>12</sub>H<sub>22</sub>O<sub>11</sub>) [26], and by growing granular a-C thin-films by using the EBID technique [27]. Mixtures of all a-C materials with sulfur (Aldrich Chemical Company, Inc., Rehovot, Israel) in a weight ratio of 2:1 (for commercial or films) and 10:3 (for pyrolytic) were pressed and heated for 20–24 h at 250 °C (or 400 °C) in evacuated quartz tube (assigned as a-CS).

The commercial a-C powders were structurally and chemically characterized by x-ray diffraction (XRD), SEM, and energy dispersive spectroscopy (EDS) JOEL JSM-7700 SEM. Trace elements analysis was performed by inductively coupled plasma (ICP) mass spectrometer (Perkin-Elmer (Waltham, MA, USA) ICP-OES model 3300) of acid extracts. The amorphous nature of the commercial a-C (Fisher) and a-C800 powders is shown in Figure 1. SEM images exhibit small non-crystalline grains with an average particle size of 9–10 nm. However, a tiny amount of crystalline powder cannot be excluded. EDS chemical analysis of the commercial a-C powder yields: Na (0.30(1) at %), sulfur (0.21 at %) and oxygen (2.44(1) at %) as extra elements. ICP analysis shows the presence of the non-magnetic ions: V = 2.0, Zn = 7.1, Cu = 11.1, Al = 212.7 and Na = 4625 ppm (similar to EDS), and of magnetic ions: Ni = 2.8, Mn = 133 and Fe = 360 ppm. Room temperature (RT) <sup>57</sup>Fe Mössbauer spectroscopy exhibit two magnetic sextets attributed to Fe<sub>3</sub>O<sub>4</sub> and confirm the presence of ~300 ± 50 ppm of Fe (not shown). For the fabricated pyrolytic a-C powder, although the initial Fe concentration in sucrose was <3 ppm, ICP measurements on a-CS reveal traces of element concentrations: Zn = 2.7, Al = 3.2, Ni = 4.3 and Fe 28 ppm. Due to the evaporation of carbon, the Fe amount increased by an order of magnitude but it is still lower than 360 ppm observed in the commercial a-C powder. EDS study on this a-CS showed that the average concentrations of carbon, oxygen and sulfur are: 84%, 15% and 1% respectively.

Magnetization measurements under applied dc magnetic fields (*H*) in the temperature range 5 K < *T* < 300 K were obtained by a SQUID (Quantum Design) magnetometer. Each ZFC curve was recorded after adjusting the magnetometer to be in a "real" *H* = 0 state. The FC branches were recorded either via heating (FC) or cooling (FCC) processes.

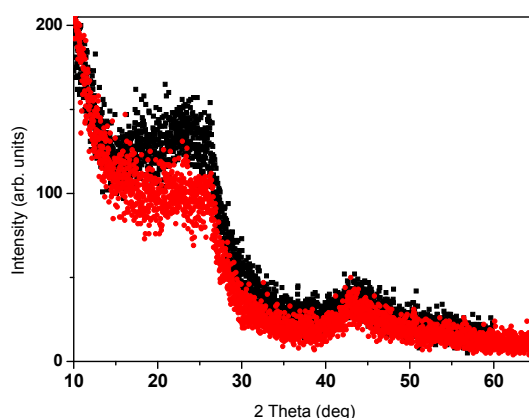


**Figure 1.** XRD patterns of commercial (Fisher) a-C (black) and a-C800 (red) powders.

## 3. Experimental Results

Extensive magnetic measurements on 21 pristine inhomogeneous commercial (Fisher) a-C samples were performed by taking 15–20 mg directly from their glass container in which they were stored for 75 years. The scattered results obtained are divided into three different groups.

- (i) Fourteen samples exhibited the magnetic features of Fe<sub>3</sub>O<sub>4</sub> and the paramagnetic (PM) impurities, as shown (for samples No. 6 and 13) in Figures 2 and 3, respectively. Due to high magnetic

transition of magnetite ( $T_M = 853$  K), the temperature dependence of the ZFC and FC plots merge at the highest measured temperature. The increase at low temperatures is related to the PM impurities. For sample No. 13 (Figure 3) after the FC process measured up to 175 K,  $H$  was switched off and the second ZFC plot was tracked. In contrast to the phenomena shown hereafter, the two ZFC curves are reproducible and overlap. In addition, Figure 3 (inset) shows the ZFC and FCC plots on another a-C commercial powder manufactured by Prolabo (9009) as Charbon R.P. Generally speaking, all Prolabo samples exhibited similar magnetic features as depicted in Figures 2 and 3 without any SC traces. The data presented hereafter are for the commercial a-C Fisher powders.

- (ii) Three a-C samples have shown SC traces around 33 K and/or 65–67 K.
- (iii) Four samples have exhibited at low  $H$  well-distinguished magnetic peaks at 50–85 K.

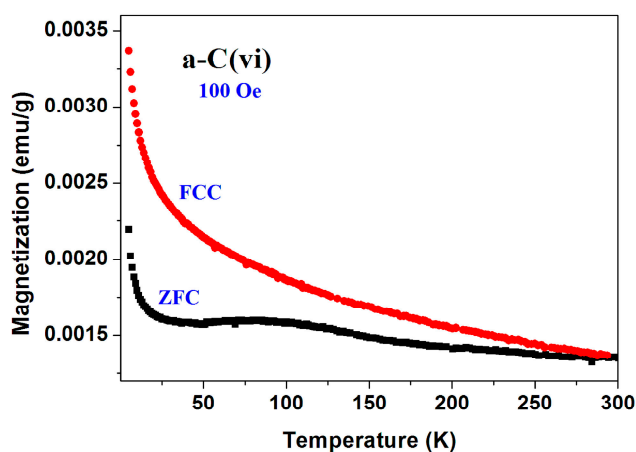


**Figure 2.** The temperature dependence of the ZFC and FC plots measured at 100 Oe up to RT of commercial a-C (No. 6) sample. The two curves merge around 300 K.

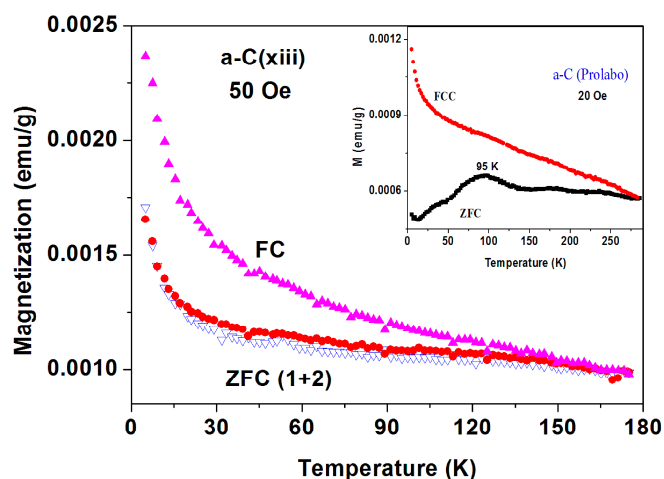
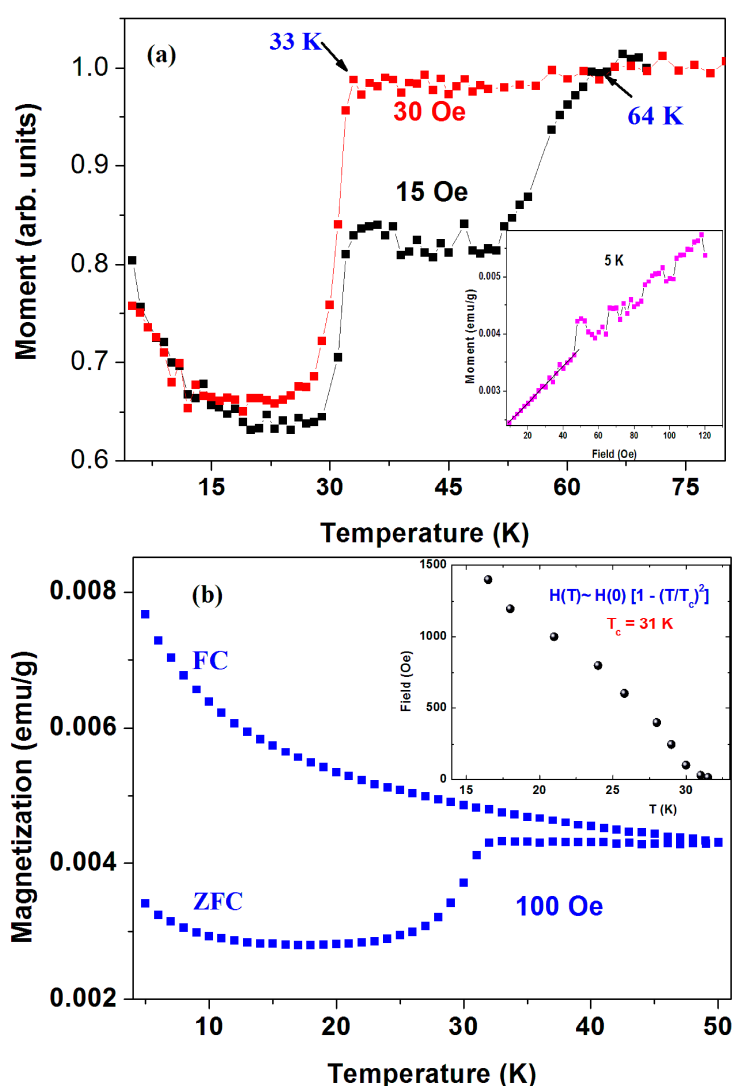


**Figure 3.** The temperature dependence of the ZFC and FC plots measured at 50 Oe of commercial a-C (sample No. 13) sample. Note the reproducibility of the ZFC process. The inset shows the data obtained for “Prolabo” a-C powder.

### 3.1. Superconductivity

(1) *a-C commercial powders.* Figure 4a shows two ZFC plots (normalized at 70 K) of the pristine a-C powder (sample No. 1) measured at  $H = 15$  and 30 Oe. The 15 Oe curve shows two drops at 33(1) K and  $T_c = 64$  K(1) attributed to two SC transitions. The estimated shielding fraction (SF) below 30 K

is ~0.03%. No corrections for the PM impurity contributions were made. Due to the inhomogeneous a-C powder, this SF value provides the lower limit for the SC volume fraction. Since the a-C powder contains 0.21 atom % of sulfur, we tend to believe that the two SC phases stem from two different a-CS phases. Due to their lower SF fractions, all attempts to isolate them and/or to determine their compositions were unsuccessful. The signature of SC at  $T_c = 64$  K is barely observed at  $H = 30$  Oe and washed out at higher applied fields. On the other hand, as expected, the lower  $T_c$  transition shifts with  $H$  (up to 1.5 kOe) to lower temperatures as shown in Figure 4b (inset). For  $H > 1.5$  kOe, the PM magnetite impurities obscure this SC transition. Below 1.5 kOe, the variation of  $T_c$  (or  $H_{C2}$ ) with  $H$  follows the conventional BCS relation:  $H_{C2} \sim [1 - (T/T_c)^2]$  where  $T_c = 31$  K obtained as free parameter. Since the SC transition is not visible at higher fields, no determination of  $H_{C2}(0)$  was done. Due to  $Fe_3O_4$  and PM impurities, further characteristic parameters of the lower SC states were not evaluated. The amorphous nature of the nano-size a-C particles, we could not press the powder into pellets and therefore no resistivity and STM studies could be performed.



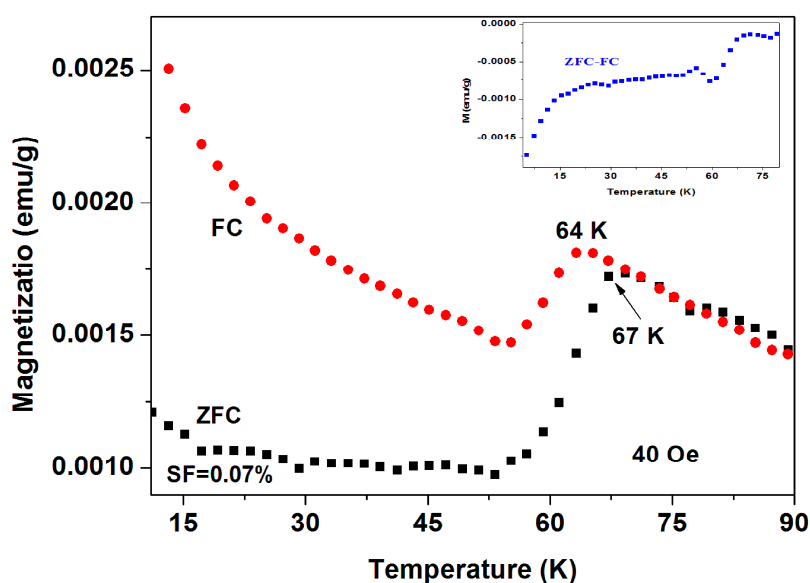
**Figure 4.** (a) ZFC curves of commercial (Fisher) a-C powder (sample No. 1) measured at 15 and 30 Oe; The ZFC and FC plots measured at 100 Oe up to 50 K are shown in (b). The insets show the low field isothermal magnetization at 5 K (a) and the variation of  $H_{C2}$  with the applied field (b).

Figure 4a (panel inset) also shows the isothermal magnetization  $M(H)$  curve at 5 K in which a linear increase up to ~50 Oe and instabilities at higher fields are observed. Due to the presence of

~350 ppm of  $\text{Fe}_3\text{O}_4$ , we assume that the linear  $M(H)$  part is a superposition of the negative Meissner contribution of the SC phases and the positive linear shape of magnetite. Therefore, these instabilities presumably express the magnetic flux line penetration above  $H_{C1}$  ~50 Oe of the SC phases. A similar curve at 10 K yields  $H_{C1}$  of 40 Oe.

Figure 4b also shows the ZFC and FC branches for this sample measured at 100 Oe up to 50 K. The SC transition around 33 K is readily observed in the ZFC branch only. At low temperatures, both branches decrease with temperature and adhere closely to the PM Curie-Weiss (CW) law:  $\chi(T) = \chi_0 + C/(T - \theta)$ , where  $\chi_0$  is the independent part of the susceptibility,  $C$  is the Curie constant, and  $\theta$  is the CW temperature. The PM parameters deduced for the FC curve are:  $\chi_0 = 4 \times 10^{-5}$  emu/g Oe,  $C = 4.3 \times 10^{-4}$  emu·K/g Oe and  $\theta = -5.8(2)$  K, which correspond to  $0.016 \mu_B/C$  atom.

The two SC phases at  $T_c = 34(1)$  K and  $T_c = 64(1)$  K were also observed separately in other a-C systems. The SC phase with  $T_c = 34$  K was obtained in a-C thin-films and presented later and the highest  $T_c = 64$  K phase was observed in another a-C commercial sample (No. 18) as shown in Figure 5. Here, the ZFC and FC plots (measured at 40 Oe) show distinct SC transitions at  $T_c = 67$  K and 64 K respectively. The SF = 0.07% deduced is twice as much as that of the previous sample, but still too low to determining the SC phase composition. This  $T_c$  is highest achieved for all a-C powders reported here. In order to reduce the magnetic contributions of magnetite and the PM impurities, we show in (Figure 5 inset) the ZFC-FC plot which becomes almost zero around 65 K. The low temperatures FC branch can be fitted with the CW law with almost similar parameters.



**Figure 5.** ZFC and FC curves of another commercial a-C powder (No. 18) measured at 40 Oe, with  $T_c = 67(1)$  K. This is the highest  $T_c$  achieved among all a-C materials. The ZFC-FC plot is shown in the inset.

*Commercial a-C reacted with sulfur at 250 °C (a-CS).* As stated above, EDS studies showed that the pristine a-C material contains ~0.21 at % of sulfur. Bearing in mind that sulfur is essential for the SC state, an attempt to increase its content was made by mixing commercial a-C powders with sulfur (ratio 2:1) and heating the mixtures at 250 °C. It appears that also the synthesized a-CS products are inhomogeneous. That means that parts taken from the same synthesized batch may exhibit different magnetic behavior. Two a-CS samples (out of many) have shown SC signatures as follows.

First, a-CS sample shows a clear SC transitions in both ZFC and FC branches at  $T_c = 38(1)$  K. EDS measurements on this a-CS sample show that the sulfur content was increased to ~10.3 at %, whereas practically no change was detected for all other element concentrations. The ZFC and FC (measured at 50 Oe) and the remnant magnetization ( $M_{\text{rem}}$ ) plots are presented in Figure 6.  $M_{\text{rem}}$  was recorded after tracing the FC curve up to 50 K, cooling the sample down to 5 K, and switching off  $H$  to zero [3].

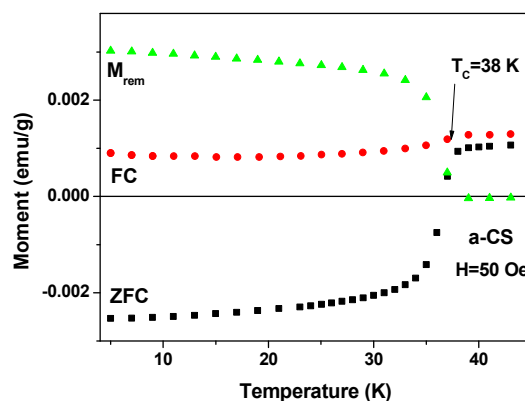


**Figure 6.** ZFC, FC measured at 50 Oe and the remnant magnetization ( $M_{rem}$ ) of a-CS. The  $Fe_3O_4$  contribution was subtracted from all three branches.

The pronounced step-like features in both ZFC and  $M_{rem}$  clearly indicate the existence of a type II SC state below  $T_c = 38 \pm 1$  K. The estimated SF = 0.15% is higher than that obtained for pristine a-C (Figure 4) and as a result the ZFC curve is in the negative region. Due to this higher SF, a drop at  $T_c$  (the Meissner effect), though smaller in magnitude, is well observed in the FC branch. This drop supports the claim for bulk SC in a-CS.

(2) *Fabricated Pyrolytic a-C powder.* In contrast to the commercial a-C powder, this a-C powder was fabricated by a multi-stage pyrolytic heat treatment of pure sucrose. Here again, XRD pattern and SEM images confirmed the amorphous nature of this powder and its ZFC and FC plots (blank) are depicted in Figure 7 (inset). This powder is basically diamagnetic. The low temperatures PM behavior is induced by tiny amount of impurities. The PM parameters values deduced for the ZFC branch by applying the CW law are:  $\chi_0 = -4.4 \times 10^{-7}$  emu/g Oe,  $C = 8.32 \times 10^{-6}$  emu K/g Oe and  $\theta = 0.16$  K. The deduced PM effective moment is  $\sim 0.007 \mu_B/C$ , a value which is an order of magnitude lower than that for pristine commercial a-C.

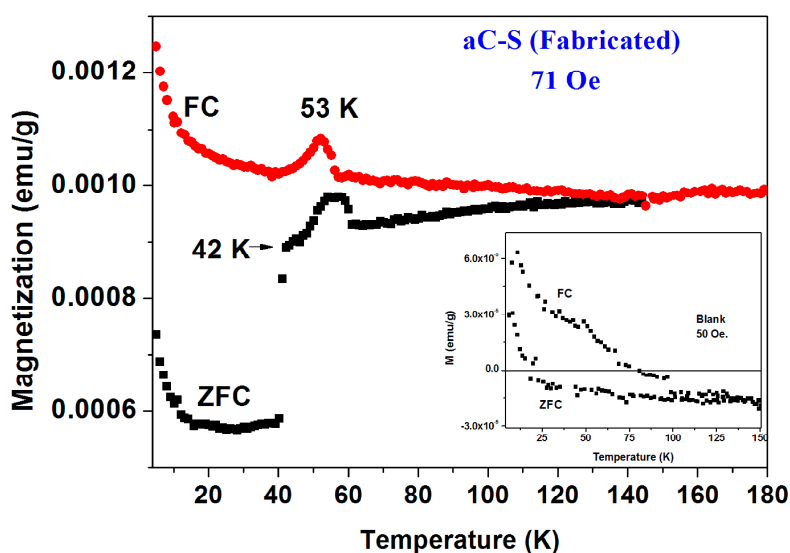


**Figure 7.** ZFC and FC curves measured at 71 Oe of a pyrolytic a-CS powder obtained after heating at 380 °C. The inset shows the almost diamagnetic behavior of the pyrolytic blank a-C material.

The a-CS materials were obtained by mixing this fabricated a-C powder with sulfur and heated the mixture at 250 °C and/or 380–400 °C under a protective atmosphere. Extensive magnetic measurements have been performed on many pyrolytic a-CS powders which appear to be not

homogeneous and exhibits magnetic scattered results. Similar to the commercial powders, the a-CS examples may be divided into three groups. (i) Most of the samples have shown the similar magnetic behavior as presented in Figures 2 and 3; (ii) One a-CS sample (obtained at 250 °C) showed a sign of a SC phase at  $T_c = 17$  K (not shown); (iii) The rest exhibited pronounced peaks at 50–60 K in their first ZFC curves as described later. A second stage of heating at 380 °C for 3 h, yields a SC phase at  $T_c = 42$  K its SF is around 0.02% (Figure 7). The lower positive PM moments are caused by PM impurities. The peaks at 53 K in both ZFC and FC branches (Figure 7) are related to the spontaneous magnetic order of solid oxygen which apparently has been detected by the EDS studies. It is important to note that the presence of oxygen appears as peaks in **both** ZFC and FC branches [28].

(3) *Superconductivity in a-C thin films.* As a third example, we present here the magnetic data collected on a-CS thin films. Six a-C thin films were grown by the EBID method (blank) and show a positive constant magnetization. This clean system is a result of the absence of PM and/or magnetite impurities. The blank films were treated with sulfur at 250 °C and two of them exhibit SC traces [27]. First, a-CS film exhibits a clear SC transition at  $T_c = 34.4(0.5)$  K (Figure 8), where  $H$  was applied perpendicular to the film area. The ZFC and FC plots were obtained after subtracting the blank magnetization. It is readily observed that below  $T_c$ , both the ZFC and FC magnetization curves are diamagnetic and the FC curve exhibit the typical expulsion of the field lines (the Meissner effect).  $T_c$  shifts with  $H$  (up to 2 kOe) to lower temperatures with a rate of  $dH/dt = 0.45$  kOe/K (not shown). The blank films contain W inclusions embedded in the a-C matrix. These inclusions are not responsible to the SC state, since SC appears only after the sulfur treatment. They only enhance the phase coherences by Josephson coupling of nearby localized SC regions. Figure 8 (inset) shows two typical isothermal hysteresis loops. Below  $H_{C1}$  at ~600 and ~400 Oe for  $T = 5$  and 10 K, respectively the  $M(H)$  curves are linear.

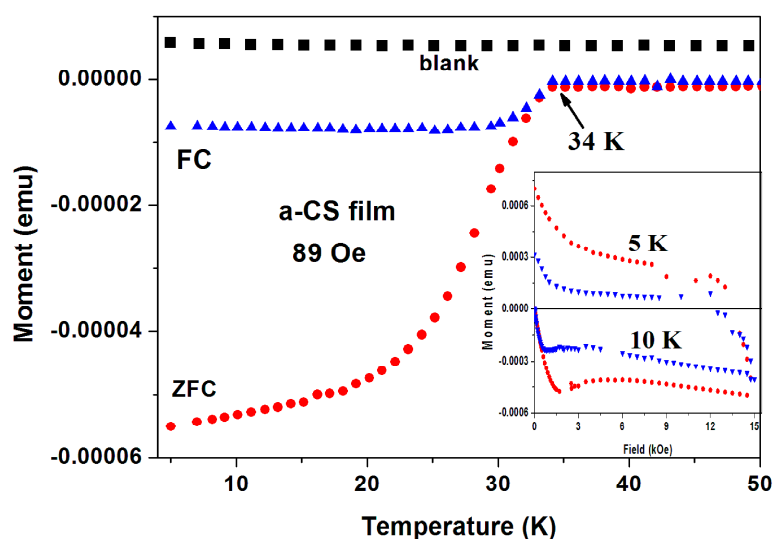


**Figure 8.** ZFC and FC branches of a-CS thin film measured at  $H = 89$  Oe perpendicular to the film surface. The  $M(T)$  plot of the blank a-C film (black) is also shown. The inset exhibits two typical isothermal  $M(H)$  plots at 5 and 10 K, confirming conclusively the SC state in this film.

Thus, in addition to the *commercial* a-C and a-CS samples (Figures 4–6), The SC state observed in the *pyrolytic* a-CS powders and in a-CS thin films were induced by sulfur. This definitely proves our claim that various a-CS phases are the origin of SC in all a-C materials studied.

### 3.2. Unusual Magnetic Properties

Thermal irreversibility in dc magnetic measurements at constant dc field ( $H$ ) is a well-known common phenomenon. It is readily found in FM, antiferromagnetic (AFM), spin-glass systems and in

SC materials as well. In all standard cases, the FC curves lie above the ZFC curves (FC > ZFC) up to a typical characteristic transition temperatures attributed to the various physical states.

The unusual magnetic behavior where the FC branches cross the ZFC curves (ZFC > FC) has been recently observed in two unrelated materials: in (i) inhomogeneous commercial and fabricated a-C and a-CS [4] and (ii) in a chiral-based magnetic memory device its structure and electrical properties are reported in Ref. [29]. Unexpectedly, in a-C and a-CS, two anomalies are observed. (1) Pronounced peaks at 50–80 K are observed in the ZFC branches only. Around the peaks position, (in contrast to the usual behavior), the ZFC branches lie above the FC curves (ZFC > FC) (puzzle 1); (2) This unusual behavior is irreproducible and disappears in the second ZFC run (puzzle 2). These two phenomena are intrinsic properties of the a-CS materials and are connected to each other. They are not ascribed neither to conventional FM nor to any magnetic impurities such as magnetite and/or oxygen. We present here the most unexpected magnetic results appearing in both commercial and fabricated a-C and a-CS materials, starting with the commercial a-C800.

(i) *Magnetic studies of commercial a-C samples:* Around 200 mg of the commercial a-C powder was heated at 800 °C under ambient conditions (a-C800). At that temperature, the amorphous carbon particles were evaporated and the residue contained mainly inorganic impurities. The ZFC and FC plots for a-C800 measured at 100 Oe are shown in Figure 9. It is observed that this material is composed of two magnetic phases: (i) The FM-like feature with a sharp transitions at 123(1) K in both branches (the Verwey transition) which are related to the presence of ferri-magnetically  $\text{Fe}_3\text{O}_4$  as deduced from both ICP and Mössbauer spectroscopy studies discussed above. The Verwey transition is attributed to electron hopping between the octahedral sites of  $\text{Fe}^{2+}$  and  $\text{Fe}^{3+}$  ions in  $\text{Fe}_3\text{O}_4$ . The bifurcation of the ZFC and FC curves at RT is caused by  $\text{Fe}_3\text{O}_4$  ( $T_M = 853$  K) as discussed above. The narrow hysteresis loop measured at 10 K (Figure 9 inset) confirms this interpretation; (ii) At low temperatures, the ZFC branch exhibits the typical PM shape and by using the CW law we obtain:  $\chi_0 = 1.7 \times 10^{-6}$  emu/g Oe,  $C = 3.24 \times 10^{-5}$  emu K/g Oe and  $\theta = -0.5$  K. Extrapolation of these values to high temperatures yields the curve assigned as PM in Figure 9, which is well below both ZFC and FC curves. This PM curve serves as a background to all other commercial a-C materials shown below.

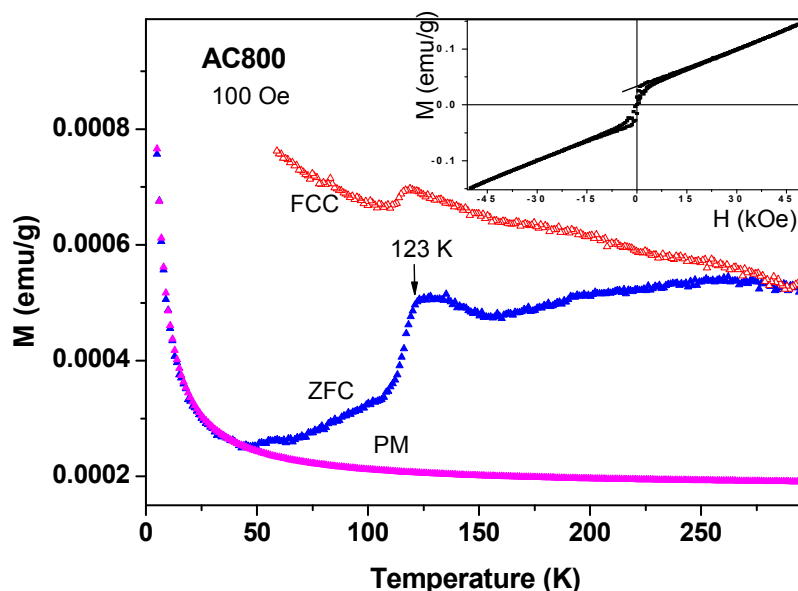


**Figure 9.** ZFC, FC and PM branches for a-C powder heated to 800 °C measured at 100 Oe and the hysteresis loop at 10 K (inset).

Four pristine commercial a-C samples have exhibited pronounced peaks at 65–85 K in their ZFC branches and a typical behavior for sample No. 6 is shown in Figure 10. The ZFC plot demonstrates

a pronounced peak at 80 K and the FC branch lies above ZFC one in the entire temperature range. The ZFC peak position is field dependent and shifts with  $H$  to higher temperatures (Figure 10 inset). For  $H = 5$  kOe, the peak obtained is at 87 K. That means that after each ZFC measurement up to room temperature, the field was switched off and turned on at 5 K to trace the next plot.

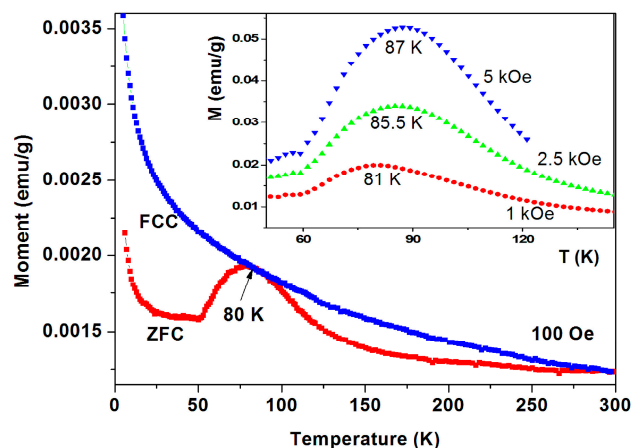


**Figure 10.** ZFC and FC curves for a-C powder (No. 6). The ZFC curve lies below the FC one. The ZFC field dependence peak position is exhibited in the inset.

Peaks at  $T \sim 50$ – $60$  K may originate from adsorbed oxygen [18]. Indeed, solidified oxygen traces are already observed (see Figure 7) but the peaks in Figure 10 cannot be attributed to oxygen because (i) they appear at much higher temperatures; (ii) Solidification of oxygen appears in **both** ZFC and FC curves (Figure 7) and (iii) the peaks related to oxygen are small and negligible as compared to the major magnetization peak (see later). Therefore, these peaks are believed to be intrinsic to the a-C powder which contains another magnetically unpaired localized spins active phase. As a result, the magnetic behavior of the pristine a-C samples is composed of three sources:  $\text{Fe}_3\text{O}_4$  and the PM impurities which are responsible for the low temperature rise (as discussed above), and an unknown additional intrinsic magnetic phase which does not exist in crystalline carbon as shown later. Note that the peak amplitude in Figure 10 is higher than that of a-C800 (Figure 9). Therefore, the Verwey transition around 120 K is not visible. Another pristine a-C sample (No. 5) shows that in a certain range of temperatures the ZFC curve lies above the FC one (Figure 11). This is a rare phenomenon which is more pronounced in the a-CS materials synthesized at  $400^\circ\text{C}$ , as presented below.

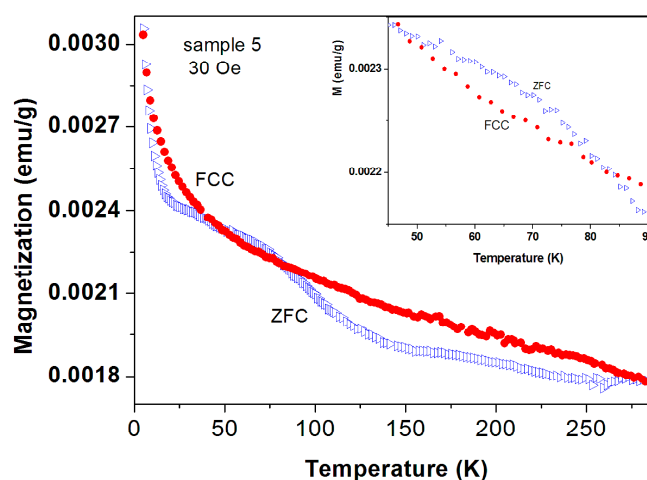


**Figure 11.** ZFC and FC branches of commercial a-C powder (No. 5) measured at 30 Oe. The ZFC curve lies above the FC one. The inset extends the temperature range in which this phenomenon occurs.

(ii) *Magnetic studies of a-CS samples synthesized at 400 °C.* The Traces of SC phases in a-C and in a-C synthesized with sulfur (a-CS) at 250 °C discussed above motivated us to explore a-CS materials which were synthesized at 400 °C. Several a-CS samples were synthesized. Since the a-C powder is not homogeneous, it may be expected that synthesis at elevated temperatures would produce better homogeneous products. It appears, however, that all synthesized samples remain inhomogeneous. In what follows, the magnetic properties of two a-CS parts (part I and III) taken from the **same** batch of sample 1 are described. Part II exhibited similar magnetic behavior to that shown in Figure 2. EDS study of this a-CS sample shows that the sulfur content increases to 0.69 at %, a value which is a bit higher than 0.21 at % obtained for pristine a-C powder, but much smaller than that of a-CS sample synthesized at 250 °C.

*Sample 1 part I.* The ZFC and FC curves measured at  $H = 100$  Oe and 1 kOe are presented in Figures 12 and 13. The magnetic irreversibility up to RT, and the peak in ZFC( $T$ ) at 78 K can easily be seen. Due to the high ZFC peak, the FC branch crosses the ZFC one, (see also Figure 11) thus in this temperature range (63–106 K) we observe unexpectedly that ZFC > FC (puzzle 1). Here again, the ZFC( $T$ ) and FC( $T$ ) merging at RT is due to  $\text{Fe}_3\text{O}_4$ . Note the minor peak around 50 K which is attributed to the spontaneous magnetic order of solid oxygen as discussed above. At low temperature, the PM plot follows the CW law and the PM parameters deduced are:  $\chi_0 = 6.1 \times 10^{-6}$  emu/g Oe,  $C = 1.72 \times 10^{-5}$  emu K/g Oe and  $\theta = 0.41$  K, values which are very similar to these obtained for a-C powder. This  $C$  value corresponds to PM effective moment  $P_{\text{eff}} = 0.01 \mu_{\text{B}}/\text{C}$ . That means that the PM impurities do not change much during the 400 °C heating process. Here again, the extrapolated PM curve lies below the ZFC and FC plots. The isothermal magnetization  $M(H)$  curve measured at 5 K (Figure 12 inset) first increases linearly up to 25 kOe and then tends to saturate. This curve may be fitted as: (ii)  $M(H) = H(-\chi_{\text{d}} + \chi_{\text{p}})$ , where  $-\chi_{\text{d}} = -2.8 \times 10^{-5}$  and  $\chi_{\text{p}} = 2.7 \times 10^{-5}$  emu/g·Oe are the a-C matrix intrinsic diamagnetic and the PM ions contributions, respectively.

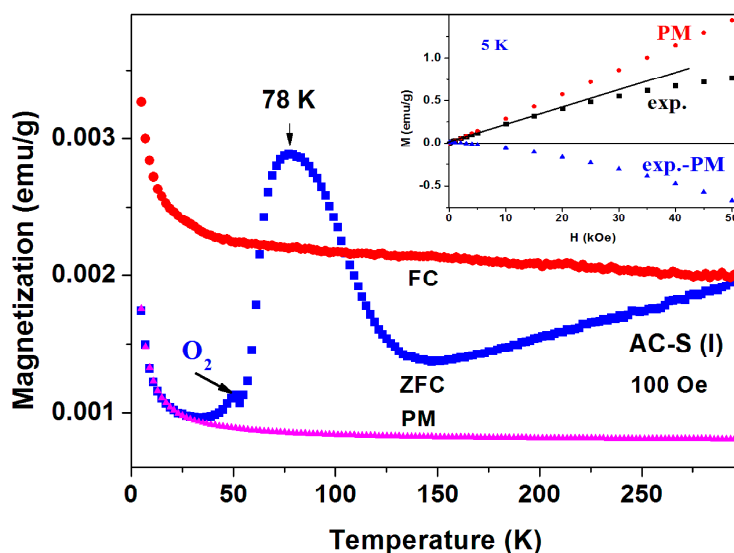


**Figure 12.** ZFC, FC and PM branches measured at 100 Oe for a-C-S (sample 1, part I) heated to 400 °C. The black arrow points to the oxygen solidification contribution. The inset shows the experimental isothermal  $M(H)$  (in black) and the linear PM contribution (in red) at 5 K.

At 1 kOe the irreversibility observed in Figure 12 disappears and both ZFC and FC curves coincide to one curve (Figure 13). The peak position is field dependent and shifts to lower temperatures with  $H$ , in contrast to Figure 10. The peaks are at: 71, 67 and 59 K for  $H = 1, 5$ , and 10 kOe, respectively (Figure 13, inset). At higher applied fields, the PM contribution masks the peaks and they are not visible.

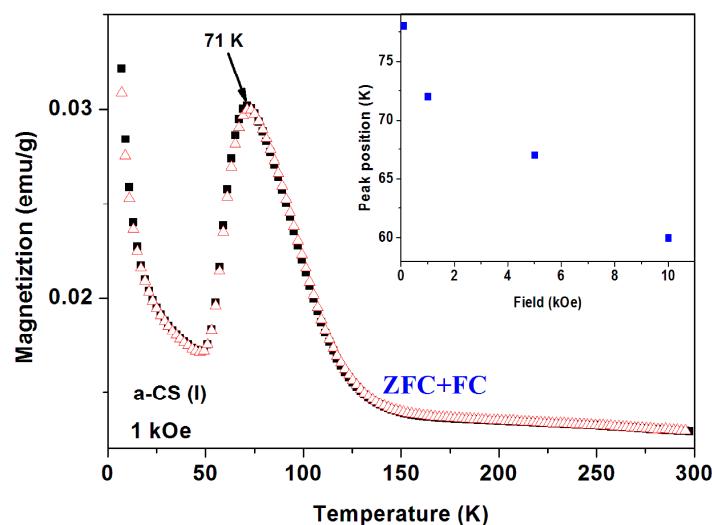


**Figure 13.** ZFC and FC branches of a-CS (sample 1, part I) measured at 1 kOe. The field dependence of the peak position is shown in the inset.

The measurements of a-CS sample 1, part III, are exhibited in Figure 14. The most striking effect is that below 150 K, the entire ZFC curve is **above** the FC one down to 5 K, whereas at higher temperatures (inset) the FC signals exceed the ZFC curves as expected. This indicates that this peculiar behavior does not stem from any experimental failure. The two ZFC > FC phenomena (Figures 12 and 14) have the same origin and the slight discrepancy may be caused by tiny differences in their inhomogeneous composition.

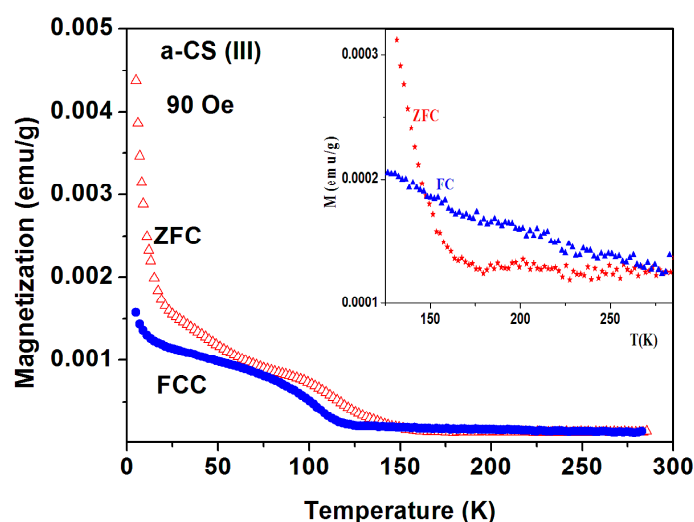


**Figure 14.** ZFC and FC branches of a-CS (sample 1, part III) measured at 90 Oe. The inset shows the normal behavior of these plots above 150 K.

*Magnetic properties of pyrolytic a-CS samples synthesized at 400 °C.* The magnetic behavior of the blank pyrolytic a-C powder was already presented in Figure 7 (inset). Several a-CS samples have been synthesized at 400 °C and the scattered results obtained are very similar to that shown above. In Figures 15 and 16, we show two examples, out of many, which definitely prove that puzzle 1 is reproducible.

*Sample 1(part III).* In order to explore the peak nature in the ZFC branch, we show in Figure 15 the measurements at 500 Oe of sample 3 (part III) where two ZFC and FC processes were performed.

The protocol of Figure 15 is as follows. (a) In order to shorten the elapsing time between the two measurements and to eliminate the PM contribution, the measurements were started at 20 K and  $H = 0$ . Then, the field was turned on to 500 Oe to trace ZFC(i) curve; (b) At 150 K, the FCC(i) (via cooling) plot was measured back to 20 K; (c)  $H$  was switched off, the SQUID was heated to RT and immediately cooled back to 20 K; (d) The field was switched back on to 500 Oe to record the ZFC(ii) up to 70 K and (e) the FCC(ii) process was completed.

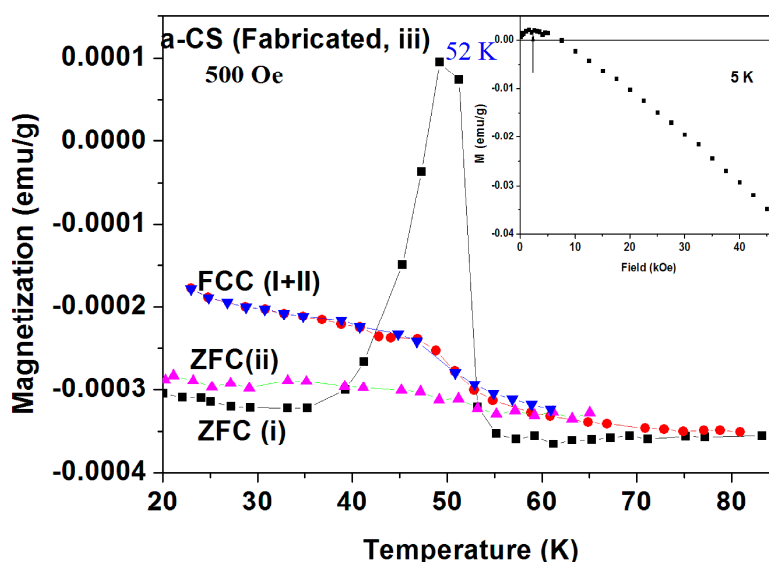


**Figure 15.** Two ZFC and FC plots of pyrolytic a-CS (sample 1 part III) measured at 500 Oe. The ZFC(i) (in black) and FCC(i) (in red) curves were measured up to 150 K and ZFC(ii) and FCC(ii) up to 70 K.

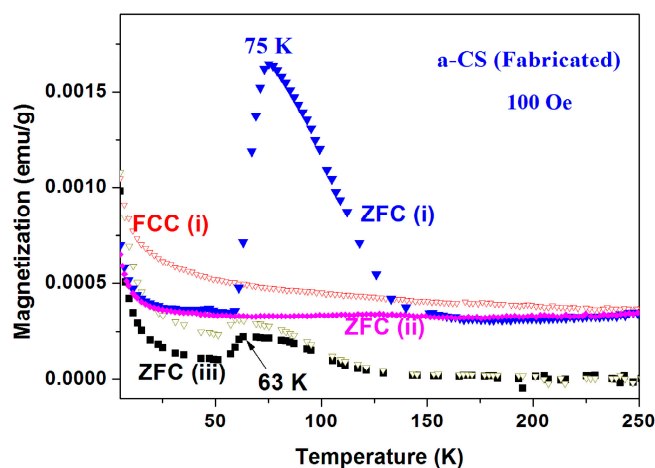


**Figure 16.** Two ZFC and FC plots of a-CS synthesized from pyrolytic a-C at 400 °C (sample 4 part III) measured at 500 Oe. ZFC(iii) was measured 1.5 years after ZFC(I) and ZFC(II). The almost diamagnetic  $M(H)$  plot at 5 K is shown in the inset.

Similar to Figure 11, the pronounced peak around 52 K in the ZFC(i) run did not show up in the FCC(i) plot which crosses the ZFC(i) one at 42 and 53 K (ZFC > FC, puzzle 1). Moreover, this peak is totally suppressed in the ZFC(ii) curve which was measured shortly later (puzzle 2). It is interesting to note that FCC(i) coincides with FCC(ii), indicating that the peak in ZFC(i) does not stem from adsorbed oxygen, and is not an experimental artifact. This also proves that the sample was not damaged and that no extra magnetization was gained during these measurements. The  $M(H)$  at 5 K of the pyrolytic a-CS sample is shown in Figure 16 (inset). Due to the small amount of magnetite and PM impurities,

$M(H)$  saturates at  $M_s = 0.0021$  emu/g and then becomes diamagnetic. This  $M_s$  value corresponds to 20.3 ppm of  $\text{Fe}_3\text{O}_4$  ( $M_s = 94.5$  emu/g) and fits well to Fe concentration accepted from ICP study reported above.

*Sample 4 (part III).* Figure 16 shows three sequences performed on another pyrolytic a-CS using the same protocol as for Figure 15. Here again, the two puzzles are present and the two FCC branches overlap. For the sake of clarity, FCC(ii) is not shown. This material was restored under ambient conditions and re-measured 18 months later. Surprisingly, a broad peak in the ZFC(iii) run re-appears at 63 K. Although this temperature is lower than 75 K, the fact that the elusive ZFC peak is restored with time is appealing.

(iii) *Magnetic studies of a-C+B and crystalline graphite.* The same two puzzles described above have been observed in a mixture of pristine a-C and boron powders (instead of sulfur) reacted at 400 °C (a-C + B). Figure 17 shows two ZFC and one FCC measured similarly to the protocol described previously. All the features described above appear here too. However, since this a-C powder contains sulfur, it is possible that this behavior is related to tiny a-CS fraction imbedded in the a-C + B matrix.

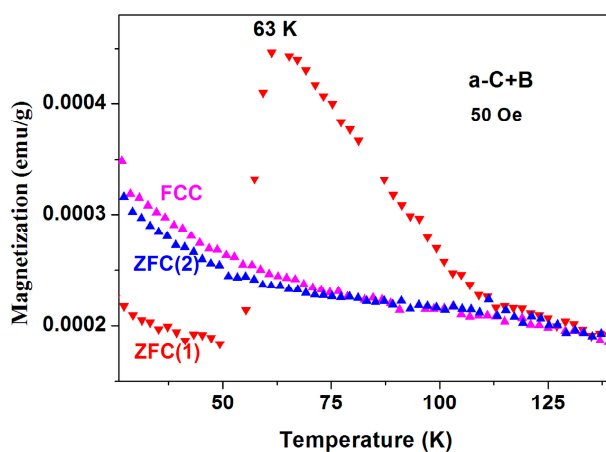


**Figure 17.** ZFC and FC curves measured at 50 Oe for commercial a-C powder synthesized with boron at 400 °C.

As a final point of interest, Figure 18 shows magnetic studies performed on a mixture of crystalline graphite (BDH) and sulfur which was synthesized at 400 °C under the same conditions described above. The magnetic impurities traces (not determined) dictate the plots shape in Figure 18. None of the two mentioned puzzles are observed here. The results obtained are consistent with recent data published on highly ordered pyrolytic graphite (HOPG) [30].

The accumulated experimental results of both inhomogeneous commercial and fabricated a-C powders (Figures 9–17) can be summarized as follows: (1) Both powders are magnetically inhomogeneous; (2) The materials and their a-CS products contain traces of  $\text{Fe}_3\text{O}_4$  and PM impurities; (3) At low applied fields, a few a-C powders reveal huge peaks in their ZFC curves at 50–80 K and their positions and relative amplitudes are sample and field dependent; (4) In a-CS, the FC curves cross the ZFC ones, (puzzle 1); (5) These peaks are present in the first ZFC(i) runs only and suppressed in the ZFC(ii) or FC processes performed very shortly later (puzzle 2); (6) This peak re-appears after 18 months (Figure 16); (7) The two puzzles are also observed in a-C + B but not in crystalline graphite; (9) The two puzzles are intrinsic properties of the a-CS materials. Even if this maximum is related to extra magnetic impurities, the mechanisms that produce such anomalies still remain unclear; (10) This complex inhomogeneity does not allow neither to measure twice the same material nor to reproduce the results even for two samples taken from the same batch. Obviously, the two puzzles are inter-related and connected to each other and it is quite obvious that the first puzzle is a direct consequence of the second one. Since these peaks appear only in the ZFC(i) plots, the following ZFC(ii) and/or the FC

branches behave “normally” as shown in Figures 2 and 3. The main problem remains as to the origin of the elusive peaks as discussed hereafter.

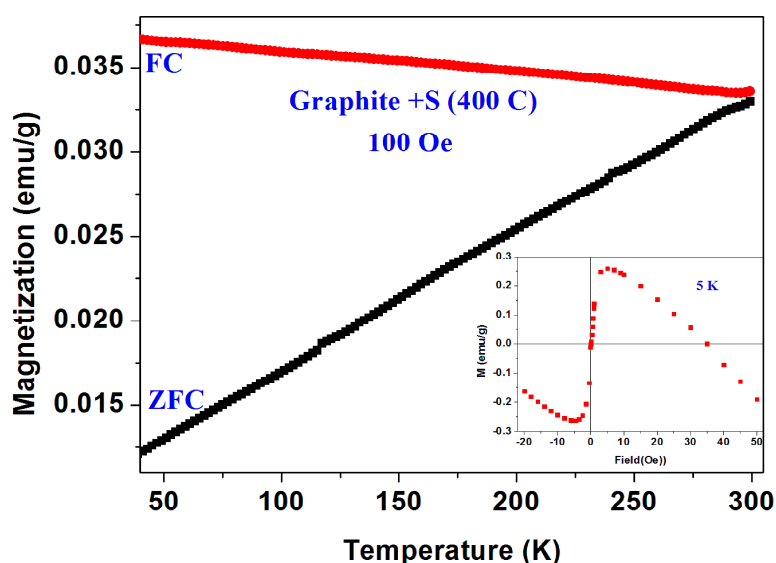


**Figure 18.** ZFC and FC curves measured at 100 Oe for crystalline graphite synthesized with sulfur at 400 °C. The isothermal  $M(H)$  plot at 5 K is shown in the inset.

#### 4. Discussion

Defect-induced magnetism in CBM may become the “Next Big Thing” in materials science, in particular, the sulfur doped porous carbons materials which have gained a great deal of attention in the last few years [31]. The above results on inhomogeneous commercial and fabricated amorphous carbon powders definitely prove the existence of: (i) traces of type II superconducting phases with  $T_c$  up to 65–67 K and (ii) two unusual magnetic phenomena rarely observed in the past. All samples contain small amounts of sulfur and it is believed that both features are due to various intrinsic a-CS phases while their structures and compositions are yet unknown. All a-C powders studied contain FM (probably  $\text{Fe}_3\text{O}_4$ ) and PM impurities, and their presence may obscure parts of the results. However, the plausible consequence is that both SC and/or peculiar magnetism are intrinsic to the a-C carbon matrix and do not arise from these impurities (or from adsorbed oxygen).

**Superconductivity.** The data presented above reveal clear evidences for type II superconducting states in a-C or a-CS powders, at  $T_c \sim 34$ –42 and  $\sim 65$  K, suggesting that these states stem from **two** different a-CS phases. Traces of the two SC phases were observed in **three** independent a-C sources. (i) A 75 year old commercial a-C powder which contains 0.21 at % sulfur (Figures 4 and 5). A reaction of this a-C powder with sulfur at 250 °C increases the sulfur concentration and the SC volume fraction by an order of magnitude although  $T_c$  remains 38 K (Figure 5). That enables to deduce the lower and upper critical fields phase diagrams and to confirm the type II SC state [3]; (ii) A diamagnetic fabricated a-C powder (sulfur-free) synthesized from sucrose [26]. However, when powder was reacted with sulfur at 250 °C and was further heated to 400 °C, traces of a SC phase at  $T_c = 42$  K was observed (Figure 7); (iii) The most convincing evidence for SC comes from a-C thin films grown by EBID which are free from PM and magnetic impurities. The reaction with sulfur at 250 °C induces a sharp SC transition at  $T_c = 34$  K and the flux expulsion in the FC branch is clearly observed (Figure 8).

The existence of these two SC phases in a-CS should be taken with a grain of salt. (i) The low SF deduced clearly indicates that the SC states observed are not bulk properties (ii) Due to the unavoidable FM and PM impurities, not all SC phases exhibit the Meissner effect; (iii) We could not press the a-C powders into pellets, therefore, it was impossible to confirm the SC states by transport and/or STM measurements; (iv) The two SC phases’ compositions are yet unknown; (v) Since only traces of the

SC phases have been detected, any attempt to classify their nature (s-type or p-type, etc.) would be misleading. However, the accumulated results presented here prove unambiguously that two SC phases with  $T_C$  up to 65 K do exist in a-C powders when doped with sulfur. We may assume that these traces support the long sought after interfacial mechanism proposed by Ginzburg in 1964 [32].

The present observations are consistent with recent results on double-wall carbon nanotubes tube DWCNT bundles, in which SC at  $T_c = 15$  K was deduced. It is assumed that that adsorbed sulfur may induce structural disorder and can locally trigger extra carriers (doping effect) into the graphite/graphene walls enhancing SC [33]. They are also consistent with a theoretical approach which claims that structural disorder, topological defects and/or foreign atoms' adsorption (S or P), may induce SC in graphite. [33] Note that in all these experiments only localized (not bulk) SC traces (low SF) were observed and that the SC transitions are significantly scattered among the different samples.

As a final point of interest, we cannot disregard the breakthrough made last year. Although HTSC was discovered in 1986, much of their SC properties remain unexplained. The last year discovery that sulfur hydrides under high pressure (200 GPa) becomes SC at  $T_c = 203$  K heightened the mystery surrounding the HTSC materials [12]. SC in  $H_2S$  was definitely proven by resistivity measurements followed by the Meissner effect. It was clearly evidenced that under high pressure  $H_2S$  decomposed to  $H_3S$  which is supposed to be the HTSC phase. The strange thing about SC in  $H_3S$  is that (unlike other HTSC) it follows the conventional BCS theory by showing a huge isotope effect. The key for SC in  $H_3S$  is the interaction between the electrons and the high frequency hydrogen vibrations of the light hydrogen atoms. We may add with some confidence that using the same token may explain the SC state in sulfur doped a-C. The relatively light nonmetallic carbon atoms (next to hydrogen in the periodic table) and their high vibration frequencies as simple harmonic oscillators induce SC even at *ambient pressure* with  $T_C$  as high as 67 K. Thus, the common denominator in both a-CS and  $H_3S$  systems is low mass atoms and sulfur which may be the basic components in new HTSC. Alternatively, it is possible that the a-C and a-CS powders contain a small amount of hydrogen (not detected by EDS) and that the observed SC states are pressed  $H_2S$  ( $H_3S$ ) embedded or adsorbed in the amorphous carbon particles. This scenario implies that a-CS and/or other CBM materials are promising candidates for discovery of new high  $T_c$  superconductors.

*Peculiar magnetic behavior.* We have observed an impressive thermal irreversibility in FC and ZFC curves of the inhomogeneous a-C powders which also contain magnetite and PM impurities. The plausible consequence is that this irreversibility does not arise from these impurities or from molecular adsorbed oxygen. In commercial and fabricated a-CS samples (synthesized at 400 °C) three unexpected reproducible magnetic phenomena are observed: (a) pronounced peaks at 50–80 K appear in the virgin ZFC branches, and around the peak positions the FC curves cross the ZFC plots (ZFC > FC, puzzle 1). This unique phenomenon is in contrast to the general trend where FC > ZFC; (b) The peaks that appear are elusive and suppressed in the second ZFC and/or FC runs performed a short time later (puzzle 2); (c) The suppressed peak re-appears after 18 months (Figures 15 and 16). These peculiarities are not observed in crystalline graphite (Figure 18). That means that these two puzzles are not accidental, but are connected to the amorphous appearance of the a-C powders. We do not have any consistent explanation for these three phenomena. Nevertheless, it is quite obvious that the first puzzle is a direct consequence of the second one. The suppression of extra magnetization gained in the first ZFC, directly affects the second ZFC and/or the FC branches which exhibit a normal behavior (FC > ZFC) as shown in Figures 2 and 3. The possibility that experimental errors and/or adsorbed oxygen is the reason for these phenomena has been excluded. Two questions remain unanswered: (i) the origin of the peaks and (ii) the reason for their disappearance after the first ZFC run.

As a hand waving explanation, we may assume that the a-CS systems are in a double-well potential state with a probability to find the system in one of the two wells. Sulfur in a-CS is distributed in an inhomogeneous manner and may induce several ordered states such as: FM or AFM, spin-glass, etc.). It may occur that in the virgin ZFCs run, the systems are trapped in one magnetic potential well state and shift to the second state in the following ZFC(ii) or FC processes. It is proposed that prior to

applying the external field the carbon magnetic moments are randomly distributed over the entire volume. The low  $H$  directs these moments to flip along its direction in a parallel FM-like manner. Above the peaks position which are sample dependent (55–80 K), the antiparallel exchange coupling is more favored and the AFM-like behavior is more preferred. As a result, in the following sequences, the net magnetic moment is lower than that of the virgin ZFC one. Note that at high  $H$  the irreversibility is absent (Figure 12) and the system behaves “normally”.

It should be noted that in addition to a-CS reported here, the magnetic peaks in the ZFC branch as well as the unusual ZFC > FC behavior were observed in three other unrelated systems: In (i) chiral-based magnetic memory device [29]; in (ii) double DWCNT in which the peak is elusive and disappears after the ZFC run [33]; and unexpectedly (iii) in liver taken from a patient with mantle cell lymphoma (Figure 19). The common denominator is that all four samples contain (a) carbon (the major component in the chiral-based magnetic memory device) and (b) a magnetic element such as Fe or Ni. The current state of experiments does not allow us to suggest any consistent explanation for the peculiar phenomena presented here. It definitely warrants further long-term, systematic experimental investigations.

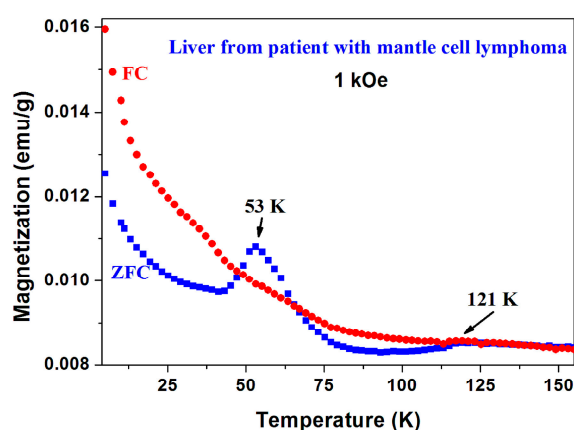


**Figure 19.** ZFC and FC curves of human liver taken from a patient with mantle cell lymphoma.

The highest SC  $T_c$  values (65 K) and the peak position in the first ZFC branches are very close to each other. Therefore, we may suggest that the extra magnetization gained in the ZFC process effectively affects the SC state formation in a way which is similar to the well-known HTSC cuprates. The present work triggers other important questions such as: the composition of the two SC phases in a-CS and the interrelation between the magnetic and SC states. Most urgent is to undertake a systematic experimental work, aiming to increase the reproducibility and to achieve bulk SC phases in a-CS.

**Acknowledgments:** We thanks to Oded Millo and Emanuel W. Prilutskiy and for supplying the a-C thin films and fabricated powders and to Yakov Kopelevich for his contribution in very beginning of this project.

**Conflicts of Interest:** The author declares no conflict of interest.

## References

1. Coletti, C.; Forti, S.; Principi, A.; Emtsev, K.V.; Zakharov, A.A.; Daniels, K.M.; Daas, B.K.; Chandrashekhara, M.V.S.; Ouisse, T.; Chaussende, D.; et al. Revealing the electronic band structure of trilayer graphene on SiC: An angle-resolved photoemission study. *Phys. Rev. B* **2013**, *88*, 155439. [[CrossRef](#)]
2. Kopelevich, Y.; Esquinazi, P.; Torres, J.H.S.; Moehlecke, S. Ferromagnetic- and superconducting-like behavior of graphite. *J. Low Temp. Phys.* **2000**, *119*, 691–702. [[CrossRef](#)]
3. Felner, I.; Kopelevich, Y. Magnetization measurement of a possible high-temperature superconducting state in amorphous carbon doped with sulfur. *Phys. Rev. B* **2009**, *79*, 233409. [[CrossRef](#)]

4. Felner, I. Superconductivity and unusual magnetic behavior in amorphous carbon. *Mater. Res. Express* **2014**, *1*. [[CrossRef](#)]
5. Hannay, N.B.; Geballe, T.H.; Matthias, B.T.; Andres, K.; Schmidt, P.; Macnair, D. Superconductivity in Graphitic Compounds. *Phys. Rev. Lett.* **1965**, *14*, 225–226. [[CrossRef](#)]
6. Weller, T.E.; Ellerby, M.; Saxena, S.S.; Smith, R.P.; Skipper, N.T. Superconductivity in the intercalated graphite compounds C(6)Yb and C(6)Ca. *Nat. Phys.* **2005**, *1*, 39–41. [[CrossRef](#)]
7. Ganin, A.Y.; Takabayashi, Y.; Khimyak, Y.Z.; Margadonna, S.; Tamai, A.; Rosseinsky, M.J.; Prassides, K. Bulk superconductivity at 38K in a molecular system. *Nat. Mater.* **2008**, *7*, 367–371. [[CrossRef](#)] [[PubMed](#)]
8. Song, L.W.; Fredette, K.T.; Chung, D.D.D.; Kao, Y.H. Superconductivity in Interhalogen-Doped Fullerenes. *Solid State Commun.* **1993**, *87*, 387–391. [[CrossRef](#)]
9. Da Silva, R.R.; Torres, H.; Kopelevich, Y. Indication of superconductivity at 35 K in graphite-sulfur composites. *Phys. Rev. Lett.* **2001**, *87*, 147001. [[CrossRef](#)] [[PubMed](#)]
10. Kubozono, Y.; Eguchi, R.; Goto, H.; Hamao, S.; Kambe, T.; Terao, T.; Nishiyama, S.; Zheng, L.; Miao, X.; Okamoto, H. Recent progress on carbon-based superconductors. *J. Phys. Condens. Matter* **2016**, *28*, 334001. [[CrossRef](#)] [[PubMed](#)]
11. Black-Schaffer, A.M.; Annica, M.; Doniach, S. Resonating valence bonds and mean-field d-wave superconductivity in graphite. *Phys. Rev. B* **2007**, *75*, 134512. [[CrossRef](#)]
12. Drozdov, A.P.; Eremets, M.I.; Troyan, I.A.; Ksenofontov, V.; Shylin, S.I. Conventional superconductivity at 203 kelvin at high pressures in the sulfur hydride system. *Nature* **2015**, *525*, 73–76. [[CrossRef](#)] [[PubMed](#)]
13. Kumari, L.; Subramanyam, S.V. Magnetoresistance and magnetic field induced metal-insulator transition in intercalated amorphous carbon. *Mater. Sci. Eng. B* **2006**, *129*, 48–53. [[CrossRef](#)]
14. Esquinazi, P.; Spemann, D.; Höhne, R.; Setzer, A.A.; Han, K.-H.; Butz, T. Induced magnetic ordering by proton irradiation in graphite. *Phys. Rev. Lett.* **2003**, *91*, 227201. [[CrossRef](#)] [[PubMed](#)]
15. Esquinazi, P.; Hohne, R.; Han, K.H.; Setzer, A.; Spemann, D.; Butz, T. Magnetic carbon: Explicit evidence of ferromagnetism induced by proton irradiation. *Carbon* **2004**, *42*, 1213–1218. [[CrossRef](#)]
16. Kopelevich, Y.; da Silva, R.R.; Torres, J.H.S.; Penicaud, A.; Kyotani, T. Local ferromagnetism in microporous carbon with the structural regularity of zeolite Y. *Phys. Rev. B* **2003**, *68*, 092408. [[CrossRef](#)]
17. Han, K.H.; Spemann, D.; Hohne, R.; Setzer, A.; Makarova, T.; Esquinazi, P.; Butz, T. Observation of intrinsic magnetic domains in C-60 polymer. *Carbon* **2003**, *41*, 785–795. [[CrossRef](#)]
18. Caudillo, R.; Gao, X.; Escudero, R.; Jose-Yacamán, M.; Goodenough, J.B. Ferromagnetic behavior of carbon nanospheres encapsulating silver nanoparticles. *Phys. Rev. B* **2006**, *74*, 214418. [[CrossRef](#)]
19. Rode, A.V.; Gamaly, E.G.; Christy, A.G.; Fitz Gerals, J.G.; Hyde, S.T.; Elliman, R.G.; Luther-Davies, B.; Veinger, A.I.; Androulakis, J.; Giapintzakis, J. Unconventional magnetism in all-carbon nanofoam. *Phys. Rev. B* **2004**, *70*, 054407. [[CrossRef](#)]
20. Arcon, D.; Jaglicic, Z.; Zorko, A.; Rode, A.V.; Christy, A.G.; Madsen, N.R.; Gamaly, E.G.; Luther-Davies, B. Origin of magnetic moments in carbon nanofoam. *Phys. Rev. B* **2006**, *74*, 014438. [[CrossRef](#)]
21. Mathioudakis, C.; Kelires, P.C. Atomistic simulations of low-density nanoporous materials: Carbon nanofoams. *Phys. Rev. B* **2013**, *87*, 195408. [[CrossRef](#)]
22. Ma'Maari, F.A.; Moorsom, T.; Teobaldi, G.; Deacon, W.; Prokscha, T.; Luetkens, H.; Lee, S.; Sterbinsky, G.E.; Arena, D.A.; MacLaren, D.A.; et al. Beating the Stoner criterion using molecular interfaces. *Nature* **2015**, *524*, 69. [[CrossRef](#)] [[PubMed](#)]
23. Djeghloul, F.; Garreau, G.; Gruber, M.; Joly, L.; Boukari, S.; Arabski, J.; Bulou, H.; Scheurer, F.; Hallal, A.; Bertran, F.; et al. Highly spin-polarized carbon-based spinterfaces. *Carbon* **2015**, *87*, 269–274. [[CrossRef](#)]
24. Karan, S.; Li, N.; Zhang, Y.; He, Y.; Hong, I.-P.; Song, H.; Lu, J.-T.; Wang, Y.; Peng, L.; Wu, K.; et al. Spin Manipulation by Creation of Single-Molecule Radical Cations. *Phys. Rev. Lett.* **2016**, *116*, 027201. [[CrossRef](#)] [[PubMed](#)]
25. Felner, I.; Prilutskiy, E. Unusual Magnetic Properties and Superconductivity in Sulfur-Doped Amorphous Carbon Powder. *J. Supercond. Novel Magn.* **2012**, *25*, 2547–2555. [[CrossRef](#)]
26. Felner, I.; Wolf, O.; Millo, O. Superconductivity in Sulfur-Doped Amorphous Carbon Films. *J. Supercond. Novel Magn.* **2013**, *26*, 511–514. [[CrossRef](#)]
27. Bandow, S.; Yamaguchi, T.; Iijima, S. Magnetism of adsorbed oxygen on carbon nanohorns. *Chem. Phys. Lett.* **2005**, *401*, 380–384. [[CrossRef](#)]

28. Ben Dor, O.; Yochelis, S.; Mathew, S.P.; Naaman, R.; Paltiel, Y. A chiral-based magnetic memory device without a permanent magnet. *Nat. Commun.* **2013**, *4*, 2256. [[PubMed](#)]
29. Wang, Y.; Pochet, P.; Jenkins, C.A.; Arenholz, E.; Bukalis, G.; Gemming, S.; Helm, M.; Zhou, S. Defect-induced magnetism in graphite through neutron irradiation. *Phys. Rev. B* **2014**, *90*, 214435. [[CrossRef](#)]
30. Kicin'ski, W.; Szala, M.; Bystrzejewski, M. Sulfur-doped porous carbons: Synthesis and applications. *Carbon* **2014**, *68*, 1–32. [[CrossRef](#)]
31. Ginzburg, V.L. Concerning surface superconductivity. *JETP* **1965**, *20*, 1549.
32. Barzola-Quiquia, J.; Esquinazi, P.; Lindel, M.; Spemann, D.; Muallem, M.; Nessim, G.D. Magnetic order and superconductivity observed in bundles of double-wall carbon nanotubes. *Carbon* **2015**, *88*, 16–25. [[CrossRef](#)]
33. Larkin, G.; Vlasov, Y. Indications of superconductivity in doped highly oriented pyrolytic graphite. *Supercond. Sci. Technol.* **2011**, *24*, 092001. [[CrossRef](#)]



© 2016 by the author; licensee MDPI, Basel, Switzerland. This article is an open access article distributed under the terms and conditions of the Creative Commons Attribution (CC-BY) license (<http://creativecommons.org/licenses/by/4.0/>).